Supporting Information

Constructing n-n junction between CoFe-LDH and NiCoP/NF as bifunctional electrocatalysts for efficient overall water splitting

Mengyuan Qin,[a] Guiyuan Ma,[a] Wenxue Tan,[a] Zunhao Fan,[a] Xing Xin[a.b*]

a. School of Material Science & Chemical Engineering, Ningbo University, Ningbo Zhejiang 315211, China

b. Key Laboratory of Advanced Mass Spectrometry and Molecular Analysis of Zhejiang Province, Institute of Mass Spectrometry, School of Material Science and Chemical Engineering, Ningbo University, Ningbo 315211, China

† Footnotes relating to the title and/or authors should appear here.

Experimental Section

Materials

Nickel (II) nitrate hexahydrate ($Ni(NO_3)_2•6H_2O$, ≥97.0%), Cobalt nitrate hexahydrate ($Co(NO_3)_2·6H_2O$, ≥97.0%), Ferrous sulfate ($Fe(SO_4)_2•7H_2O$, ≥97.0%), Sodium hypophosphite (H_2NaO_2P, AR,99%), Ammonium fluoride (NH_4F, AR), Nafion (5% w/w in water and 1-propanol, Alfa Aesar), Urea ($(NH_2)_2CO$, AR) and absolute ethanol were purchased from Sinopharm Chemical Reagent Co., Ltd. Deionized (DI) water was used in all experiments. All chemicals used in this work were of analytical reagent grade, commercially available, and used without further purification. The Ni foam (NF) was used as a substrate. The NF needs to be pretreated to remove the surface oxidation layer. Firstly, the NF was washed in an ultrasonic

bath of acetone for 20 min. Subsequently, it was soaked in HCl solution (3 M) for 20 min, and rinsed with deionized water, and ethanol for 20 min, respectively.

Materials Synthes

Synthesis of NiCoP/NF

2 mmol Nickel (II) nitrate hexahydrate ($Ni(NO_3)_2•6H_2O$, 0.596 g), 2 mmol cobalt nitrate hexahydrate ($Co(NO_3)_2•6H_2O$, 0.582 g), 10 mmol Ammonium fluoride(NH_4F, 0.37 g) and 25 mmol urea(CH_4N_2O,1.5 g) were dissolved in 40 mL H_2O and stirred 10 min to get a uniform solution. Then the solution and the treated nickel foam (1 cm × 2 cm) were put into a stainless steel autoclave lined with Teflon in 100 mL, held at 120℃ for 6 h, cooled to room temperature, and washed three times in turn with deionized water and ethanol, respectively. Then put the product in the oven to dry for 3h, the pink product can be obtained. The pink product and Sodium hypophosphite (H_2NaO_2P) were put into a tubular furnace with a mass ratio of 1:10 and heated at a heating rate of 5℃ min^{-1} to 350℃ for 2 h. Finally, black NiCoP/NF was obtained. Under the condition that other chemicals and steps remain unchanged, only $Ni(NO_3)_2$-$6H_2O$ or $Co(NO_3)_2$-$6H_2O$ is added to synthesize Ni_2P/NF or Co_2P/NF, respectively.

Synthesis of CoFe-LDH@NiCoP/NF

The CoFe-LDH@NiCoP/NF was synthesized by electrodepositing CoFe-LDH onto the NiCoP/NF nanorods in an 100 mL electrolyte containing 0.15 M $Co(NO_3)_2•6H_2O$ and 0.15 M $Fe(SO_4)_2•7H_2O$ at -1.0 V *vs*. SCE with 100 s. CoFe-LDH nanosheets were

deposited directly onto the NF substrate under the same condition for comparison. Under the same conditions, CoFe-LDH nanosheets were deposited on NiCoP/NF for comparison at 50 s and 150 s, respectively, as CoFe-LDH@NiCoP/NF-50, CoFe-LDH@NiCoP/NF-150.

Synthesis of CoFe-LDH@Ni_2P/NF and CoFe-LDH@Co_2P/NF

In the same way, the Ni_2P/NF or Co_2P/NF based electroplated CoFe-LDH was synthesized in 100 s CoFe-LDH@Ni_2P/NF or CoFe-LDH@Co_2P/NF.

Synthesis of CoFe-LDH/NF

1.5 mmol $Co(NO_3)_2$•$6H_2O$, 1.5 mmol $Fe(SO_4)_2$•$7H_2O$ and 0.20 mmol CH_4N_2O were dissolved in 50 mL H_2O and stirred 10 min to get a uniform solution. Then the solution and the treated nickel foam (1 cm × 2 cm) were put into a stainless steel autoclave lined with Teflon in 100 mL, held at 120℃ for 6 h, cooled to room temperature, and washed three times in turn with deionized water and ethanol, respectively. Then put the product in the oven to dry for 3 h, the yellow product can be obtained.

Preparation of RuO_2-modified electrode

Typically, 4 mg of commercial RuO_2 (20 wt%) was independently dissolved into 2 mL of the mixed solution containing 800 μL of water + 970 μL of ethanol+30 μL of Nafion under ultra-sonication, and then the homogeneous suspension was dropped onto the cleaned NF, termed as RuO_2 for clarity.

Electrochemical Measurements

All the electrochemical curves were carried out in a conventional three-electrode system on an CHI760 electrochemical station (Shanghai Chenhua, China). Glassy carbon electrode clamped with in situ growth of active material in nickel foam are used as working electrodes (the active area of 1×1 cm^{-2} , mass loading 1.24 mg cm^{-2})， carbon rode as the counter electrode, and the normal Hg/HgO electrode as the reference electrode. After many cyclic voltammetry tests, all polarization curves were measured in 1.0 M KOH solution with a scan rate of 5 $mV \cdot s^{-1}$. All polarization curves were corrected with iR-compensation. The solution impedance of 1 M KOH measured was 5 Ω at room temperature. All the final potentials are converted to reversible hydrogen electrodes with the conversion rate E (*vs*. RHE) =E (*vs*. Hg/HgO) +0.098V+0.059 × PH. Accurate Tafel plots of CoFe-LDH@NiCoP/NF and other related catalysts were deduced from the corresponding Koutecky-Levich plots. The electrochemical double layer capacitance (*Cdl*) of the electrode was calculated by cyclic voltammetry curve in the range of scanning rate 5, 10, 15, 20 and 25 mV s^{-1}, respectively, and the voltage was 1.13~1.23 V *vs*. RHE or 0.02-0.12 V *vs*. RHE. The ECSA value is calculated by dividing the measured double-layer capacitance by the specific capacitance of the atomic smooth material: ECSA=*Cdl*/Cs. Cs is 0.04 $mF \cdot cm^{-2}$ In the range of 0.01~100000 Hz frequency, the potential range of electrochemical impedance spectroscopy is 1.427 to 1.494V (*vs*. RHE) or 0.075 to 0.123 V (*vs*. RHE), Rct is the charge-transfer resistance across the electrode/electrolyte interface, Rs is the solution resistance, and CPE is the constant phase component. Faradaic efficiency (FE)

was calculated by the equation: FE= 4×F×n/Q, where F represents the Faraday constant, n is the moles number of totally produced O_2 or H_2, and Q represents the accumulated charges passing through the working electrode. Stability tests were carried out without iR-compensation.

The crystal structures of the obtained samples were characterized using Bruker D8 Focus Advance X-ray diffraction (XRD, diffractometer with Cu-Kα radiation, λ = 0.15406 nm, receivingslit, 0.2 mm, scintillation counter, 40 mA, 40 kV) with scattering angles of 10° to 60° 2θ range at 0.02 s^{-1}. In situ XRD tests were carried out using a special sample holder. The X-ray transmission window and current collector of the in situ XRD cell was a Be disc. Micro-structural properties were determined using HITACHI SU-70 field-emission scanning electron microscopy (FESEM) and JEOL JEM-2010 high-resolution transmission electron microscopy (HRTEM) at an accelerating voltage of 200 kV. Elemental mapping was performed using a JEOL JEM-2010F transmission electron microscope operating at 200 kV. X-ray photoelectron spectroscopy (XPS) analysis was carried out on a Kratos Axis Ultra DLD spectrometer.

Description of heterojunction computation

As shown in Fig.S11, the $E - C^{-2}$ plots of NiCoP and CoFe-LDH reveals their n-type semiconductor character. The E_{fb} of NiCoP is about -0.64 V *vs*. SCE, and the E_{fb} of CoFe-LDH is estimated to be -1.35 V *vs*. SCE. This is mainly because the ECB of n-type semiconductors is more negative by approximately 0.1 or 0.2 V than the E_{fb} [1]. The bands of NiCoP and CoFe are 1.87 and 2.47 eV, respectively. Relevant

calculations are shown in Formula 1 and 2 below:

$$E_{NHE} = E_{SCE} + 0.241\ V \quad (1)$$

$$E_{VB} = E_{CB} + E_g \quad (2)$$

Therefore, the E_{VB} and E_{CB} of NiCoP are 1.27 eV and -0.60 eV, respectively, while the E_{VB} and E_{CB} of CoFe are relatively a little more negative, which are 1.16 eV and -1.31 eV, respectively. This leads to the formation of the CoFe-LDH@NiCoP/NF interfacial n-n heterojunction.

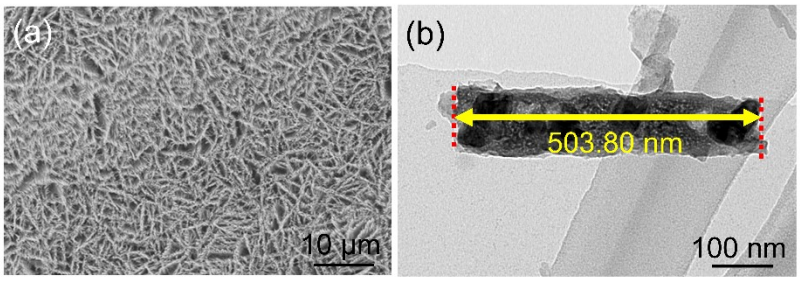

Fig. S1 (a) SEM, (b) HR-TEM images of NiCoP/NF.

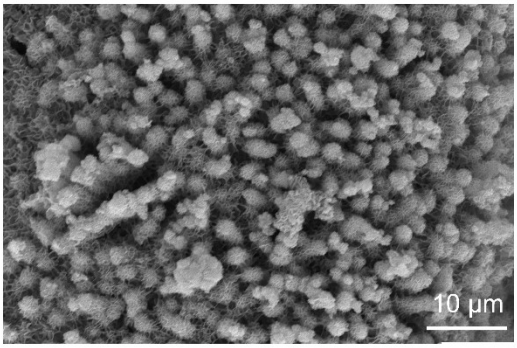

Fig. S2 SEM of CoFe-LDH@NiCoP/NF.

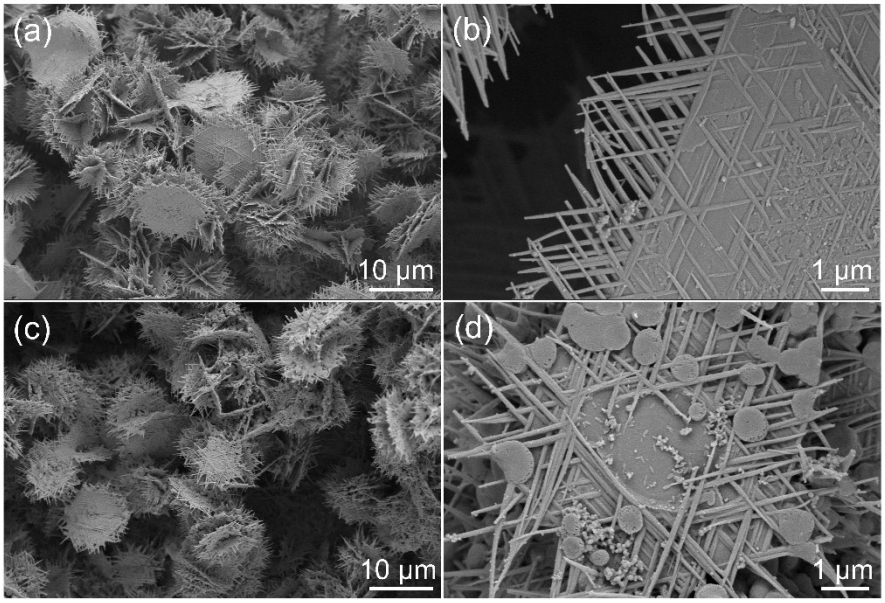

Fig. S3 SEM images of (a) and (b) CoFe-LDH@NiCoP/NF-50, (c) and (d) CoFe-LDH@NiCoP/NF-150.

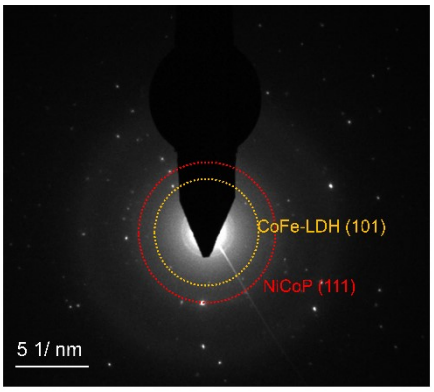

Fig. S4 SAED pattern of CoFe-LDH@NiCoP/NF.

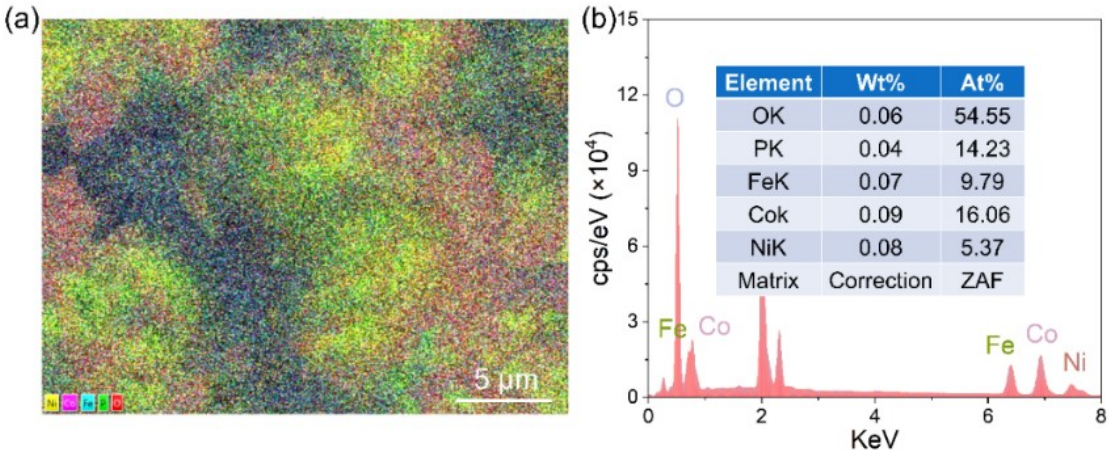

Fig. S5 EDS patterns of CoFe-LDH@NiCoP/NF sample.

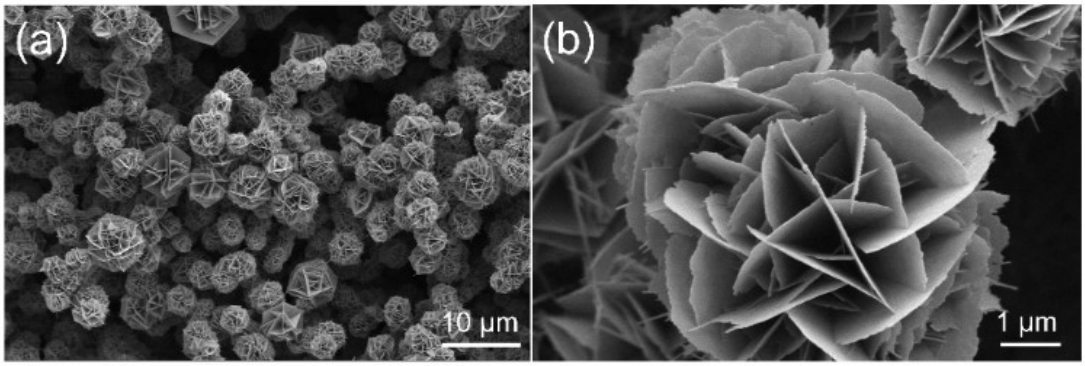

Fig. S6 SEM of CoFe-LDH/NF.

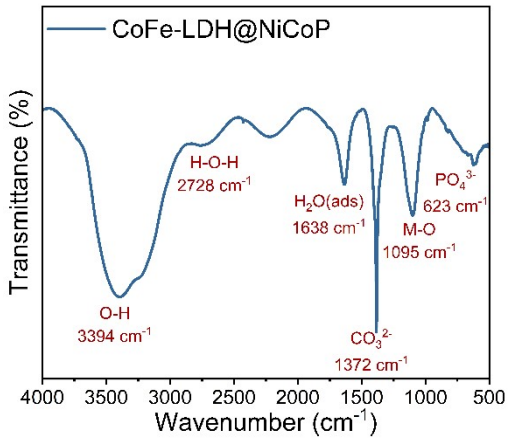

Fig. S7 FTIR spectra of CoFe-LDH@NiCoP/NF.

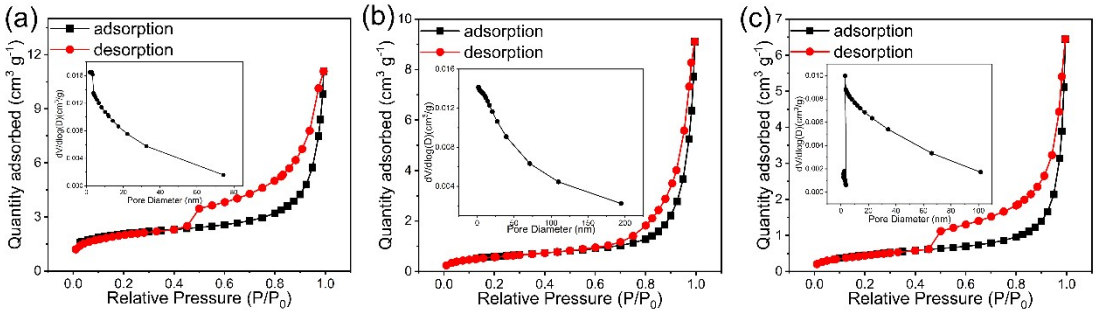

Fig. S8 N_2-adsorption-desorption isotherm curve and BJH pore size distribution curves of (a) CoFe-LDH@NiCoP/NF, (b) NiCoP/NF and (c) CoFe-LDH/NF.

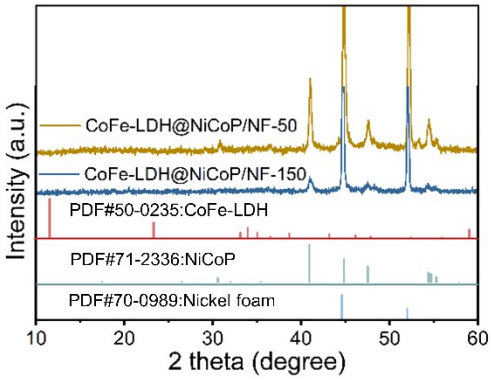

Fig. S9 XRD spectra of the CoFe-LDH@NiCoP/NF-50 and and CoFe-LDH@NiCoP/NF-150.

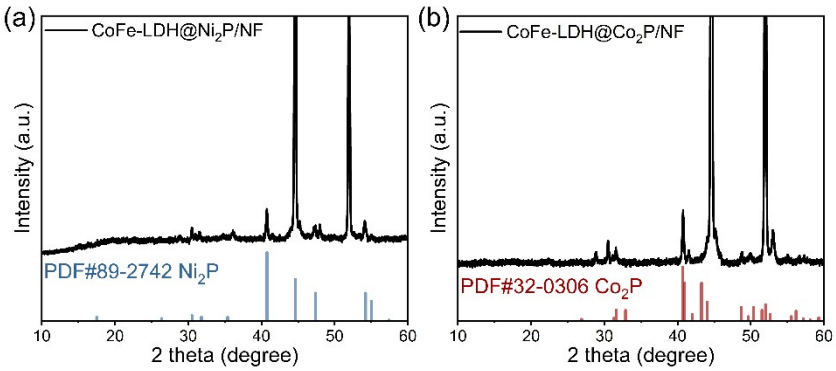

Fig. S10 XRD spectra of the (a) CoFe-LDH@Ni_2P/NF and and (b) CoFe-LDH@Co_2P/NF.

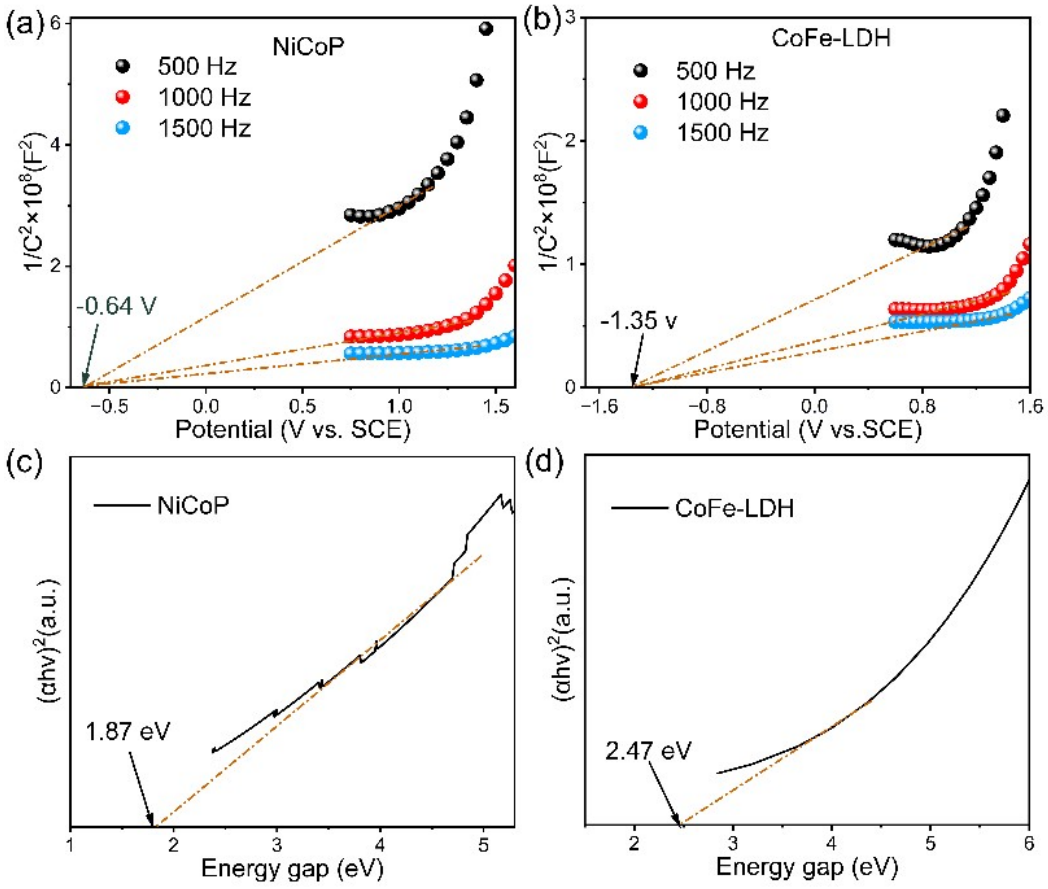

Fig. S11 M-S plots of the (a) CoFe-LDH and (b) NiCoP at various frequencies, Tauc plots of the (c) CoFe-LDH and (d) NiCoP.

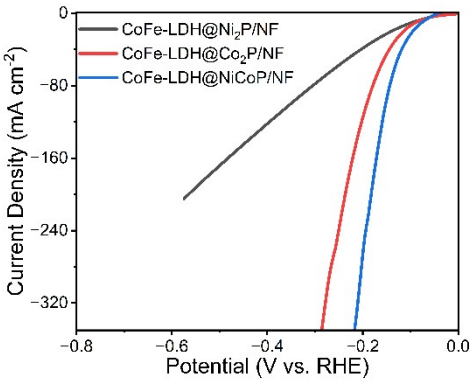

Fig. S12 LSV plots of CoFe-LDH@NiCoP/NF, CoFe-LDH@Ni_2P/NF and CoFe-LDH@Co_2P/NF in HER test.

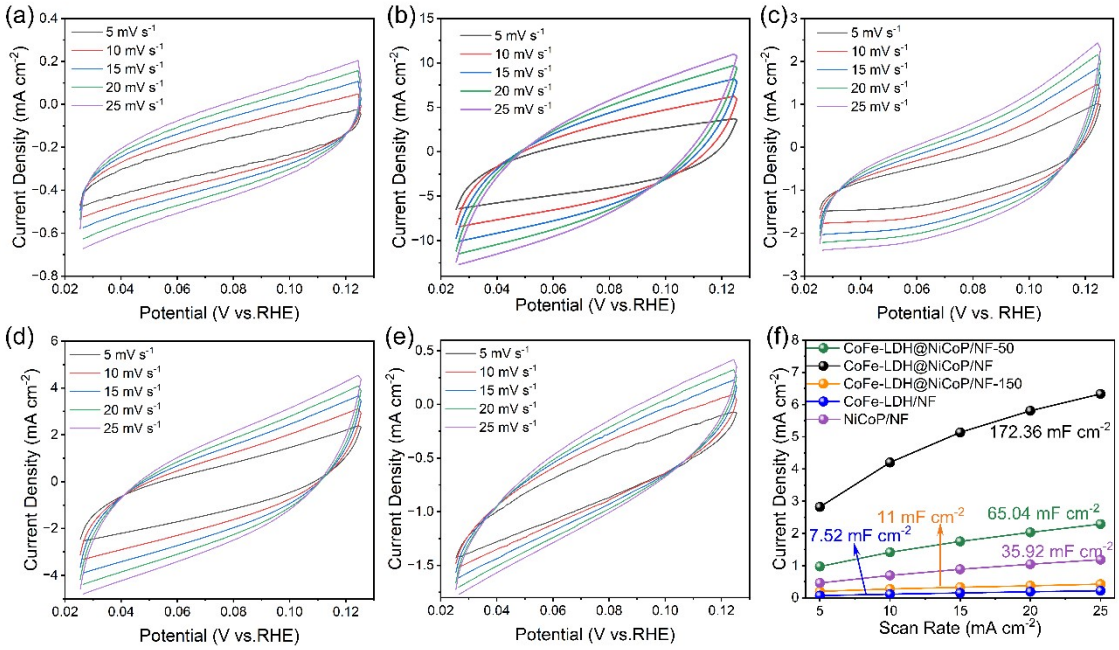

Fig. S13 Cyclic voltammetry graphs in the HER region of 0.02-0.12 V *vs*. RHE in 1 M KOH. (a) CoFe-LDH/NF, (b) NiCoP/NF, (c) CoFe-LDH@NiCoP/NF, (d) CoFe-LDH@NiCoP/NF-50 and (e) CoFe-LDH@NiCoP/NF-150, (f) Scan rate dependent Δj for the catalysts at 0.109 V *vs*. RHE.

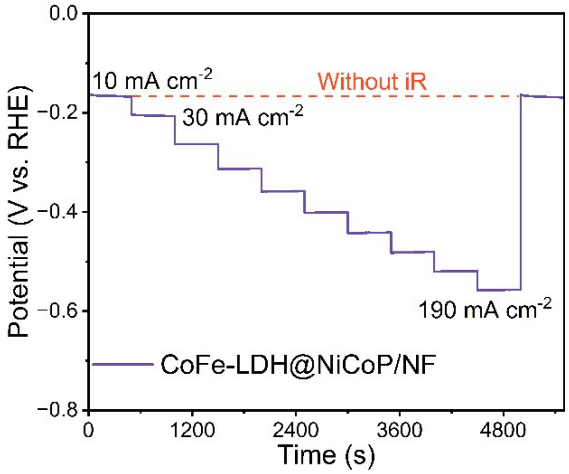

Fig. S14 Multi-currents process of CoFe-LDH@NiCoP/NF in HER tests.

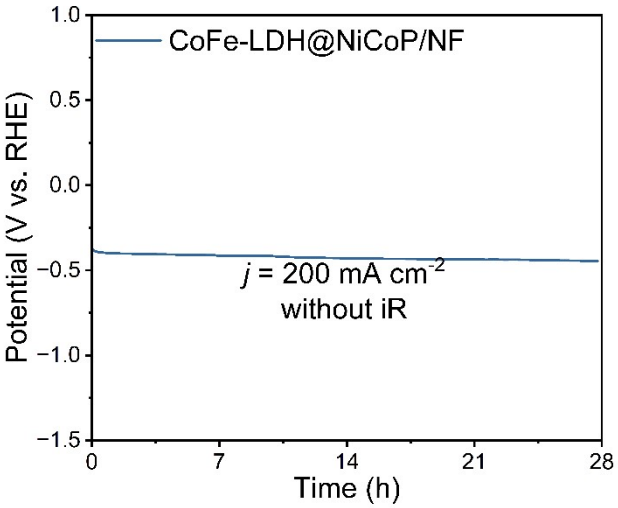

Fig. S15 chronoamperometry curves in HER process of CoFe-LDH@NiCoP/NF.

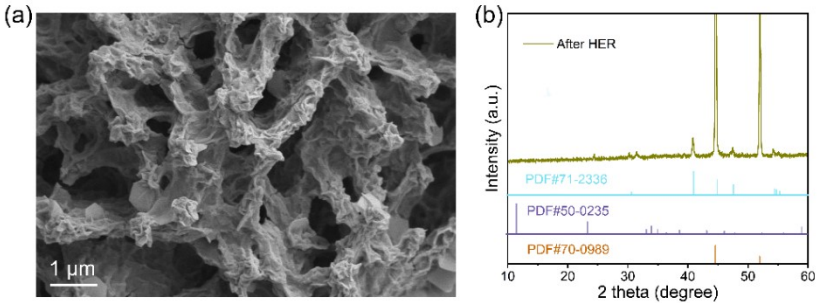

Fig. S16 (a) SEM image and (b) XRD spectra of CoFe-LDH@NiCoP/NF after HER.

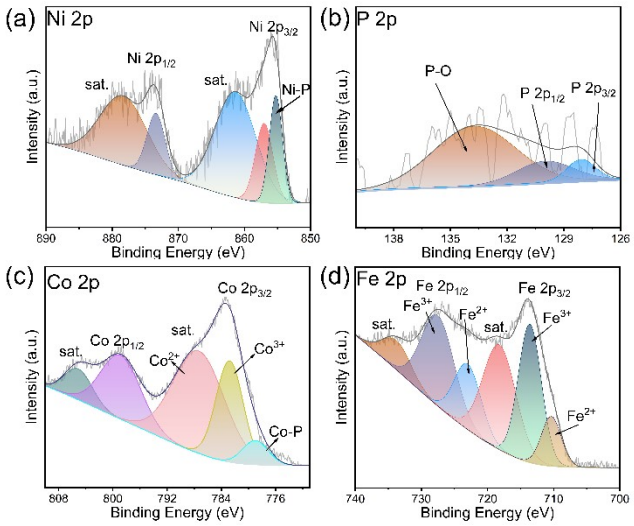

Fig. S17 The high-resolution XPS spectrum of CoFe-LDH@NiCoP/NF after HER, (a) Ni 2p, (b) P 2p, (3) Co 2p, (4) Fe 2p.

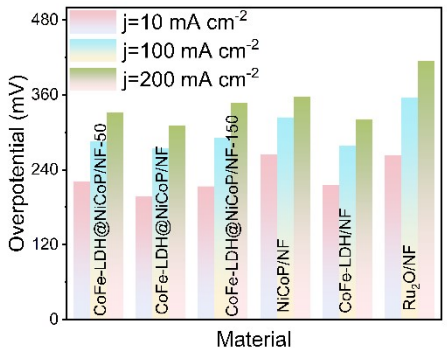

Fig. S18 Comparison of overpotentials at current densities of 10, 100 and 200 mA cm^{-2}.

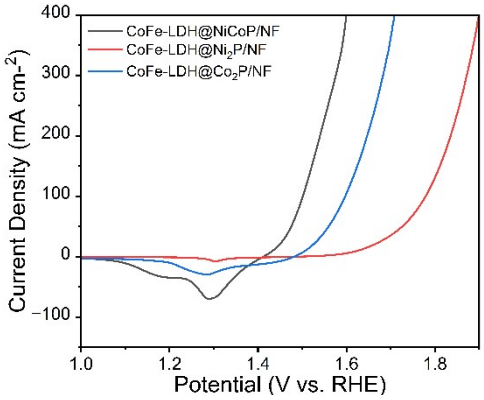

Fig. S19 LSV plots of CoFe-LDH@NiCoP/NF, CoFe-LDH@Ni_2P/NF and CoFe-LDH@Co_2P/NF in OER test.

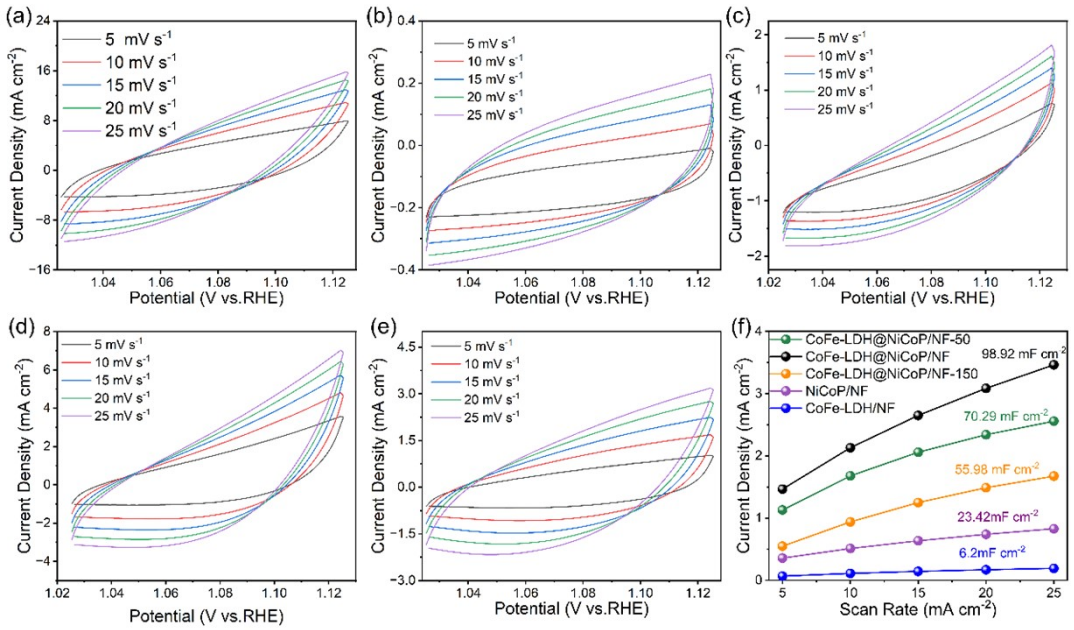

Fig. S20 Cyclic voltammetry graphs in the OER region of 1.02-1.12 V *vs*. RHE in 1 M KOH. (a) CoFe-LDH/NF, (b) NiCoP/NF, (c) CoFe-LDH@NiCoP/NF, (d) CoFe-LDH@NiCoP/NF-50 and (e) CoFe-LDH@NiCoP/NF-150, (f) capacitive ($\Delta j/2 = (ja - jc)/2$) *vs*. scan rate of as-made samples and the corresponding linear slopes.

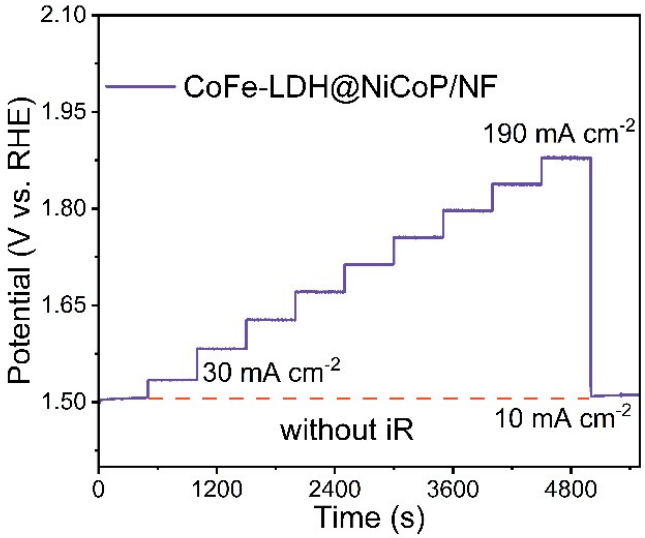

Fig. S21 Multi-current process of CoFe-LDH@NiCoP/NF in OER tests.

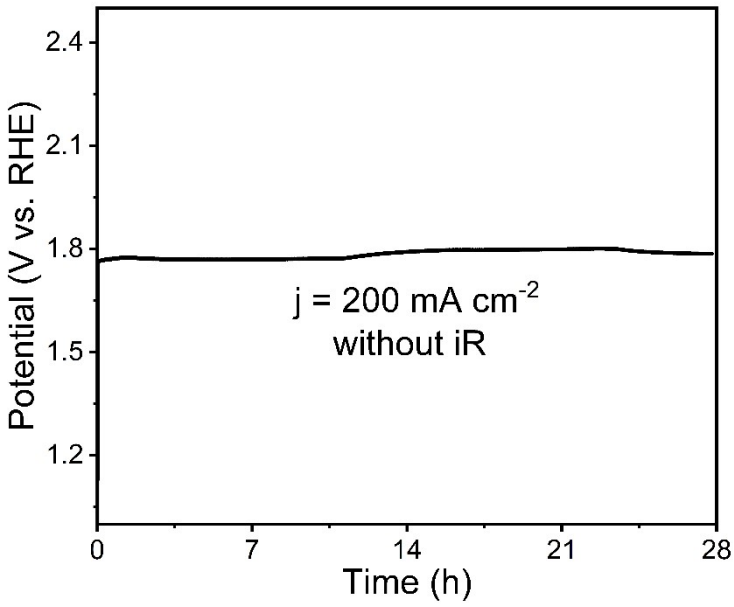

Fig. S22 Chronoamperometry curves in OER process of CoFe-LDH@NiCoP/NF.

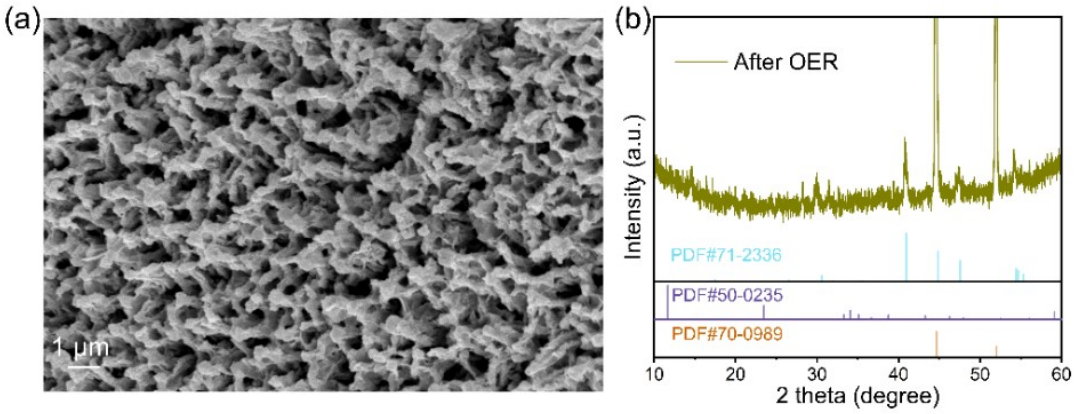

Fig. S23 (a) SEM image and (b) XRD spectra of CoFe-LDH@NiCoP/NF after OER.

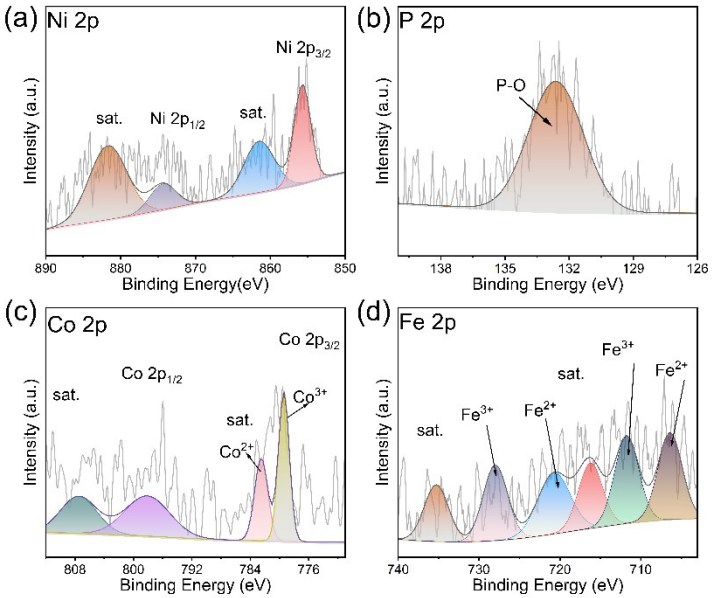

Fig. S24 The high-resolution XPS spectrum of CoFe-LDH@NiCoP/NF after OER, (a) Ni 2p, (b) P 2p, (c) Co 2p, (d) Fe 2p.

Fig. S25 a H-type gas-tight electrochemical electrolyzer (a) and (h), (b-g) H_2 and (i-n) O_2 generated at 0, 2, 4, 6, 8, 10 min.

Table S1 Overpotentials at 10 and 100 mA cm^{-2} and Tafel value of prepared catalyst in HER test.

Catalyst	Overpotential (mV) at 10 mA cm^{-2}	Overpotential(mV) at 100 mA cm^{-2}	Tafel value (mV dec^{-1})
CoFe-LDH@NiCoP/NF	75	160	53.04
CoFe-LDH/NF	141	260	104.65
NiCoP/NF	87	196	102.61
Pt/C (20%)	31	116	45.76
CoFe-LDH@NiCoP/NF-50	123	265	114.17
CoFe-LDH@NiCoP/NF-150	117	257	88.61

Table S2 Comparison of HER performance for previously reported catalysts.

Catalyst	Overpotential (mV) at 100 mA cm^{-2}	Tafel (mV dec^{-1})	Reference
This work	160	53.04	
Fe–Co–O/Co@NC-mNS/NF	201	96	[2]
N-$Co_2V_2O_7$@NF	310	56	[3]
Co/CoMoN/NF	173	68.9	[4]
$SnFeS_xO_y$/NF	167	90	[5]
HWS NiCoP/NF	220	31.34	[6]
NiCoP NWAs/NF	197	54	[7]
Mo-doped CoFe LDH/NF	227	95	[8]
NiFeCoP/NF	167.5	84.81	[9]
$NiCo_2O_4$/NiCoP	198	91	[10]
Ni_3S_2/$NiMo_2S_4$-POM/NF	338	85	[11]

Table S3 Overpotentials at 10 and 100 mA cm^{-2} and Tafel value of prepared catalyst in OER test.

Catalyst	Overpotential (mV) at 10 mA cm^{-2}	Overpotential(mV) at 100 mA cm^{-2}	Tafel value (mV dec^{-1})
CoFe-LDH@NiCoP/NF	197	275	63.02
CoFe-LDH/NF	215	279	70.25
NiCoP/NF	264	324	72.29
CoFe-LDH@NiCoP/NF-50	221	285	85.47
CoFe-LDH@NiCoP/NF-150	213	291	99.75

Table S4 Comparison of OER performance for previously reported catalysts.

Catalyst	Overpotential (mV) at 100 mA cm^{-2}	Tafel (mV dec^{-1})	Reference
This work	275	63.02	
NCFL	367	98.6	[12]
NiCoP/NF	370	116	[7]
Zn/F-NiCoP/NF	310	78.33	[13]
NiCoP@NiMn LDH/NF	293	43.7	[14]
NiCoP/CC (nest-like)	330	64.2	[15]
Mo-doped CoFe LDH/NF	331	101	[8]
CoFeV-0.25 LDH/NF	330	57	[16]
MIM-CoFe LDH	291.3	39.3	[17]
CoFeS@NiCoS	293	40.6	[18]
Cu_2S@NiFe LDHs/Cu foam	286	56.98	[19]

Table S5 Comparison of the electrolytic performance of CoFe-LDH@NiCoP/NF and representative work in recent years.

Catalyst	Potential (mV) at 100 mA cm^{-2}	Reference
This work	1.67	
N-NiCoP/NF‖N-NiCoP/NF	1.74	[20]
Er-doped CoP‖Er-doped CoP	1.9	[21]
$Fe_{0.2}NiCo_{1.8}Se_4$‖$Fe_{0.2}NiCo_{1.8}Se_4$	2.07	[22]
NiCoP‖NiCoP	1.80	[23]
Se-(NiCo)S_x/$(OH)_x$‖Se-(NiCo)S_x/$(OH)_x$	2.05	[24]
Co-Mo-P/CoNWS/NF‖CoMo-P/CoNWS/NF	1.78	[25]
Ni_3S_2/VG@NiCo‖Ni_3S_2/VG@NiCo	1.95	[26]
NiFeOH/CoS_x/NF‖NiFeOH/CoS_x/NF	1.75	[27]
Ni-250-2@NF‖Ni-250-2@NF	1.91	[28]
C@CoP-FeP/FF‖ C@CoP-FeP/FF	1.73	[29]

Reference

1 X. Li, J. Yu, J. Low, Y. Fang, J. Xiao and X. Chen, Engineering heterogeneous semiconductors for solar water splitting, *J. Mater. Chem. A*, 2015, **3**, 2485-2534.

2 T. I. Singh, G. Rajeshkhanna, U. N. Pan, T. Kshetri, H. Lin, N. H. Kim and J. H. Lee, Alkaline Water Splitting Enhancement by MOF-Derived Fe-Co-Oxide/Co@NC-mNS Heterostructure: Boosting OER and HER through Defect Engineering and In Situ Oxidation, *Small*, 2021, **17**, 2101312.

3 Z. Luo, Q. Peng, Z. Huang, L. Wang, Y. Yang, J. Dong, T. T. Isimjan and X. Yang, Fine-tune d-band center of cobalt vanadium oxide nanosheets by N-doping as a robust overall water splitting electrocatalyst, *J. Colloid Interf. Sci.*, 2022, **629**, 111-120.

4 H. Ma, Z. Chen, Z. Wang, C. V. Singh and Q. Jiang, Interface Engineering of Co/CoMoN/NF Heterostructures for High-Performance Electrochemical Overall Water Splitting, *Adv. Sci.*, 2022, **9**, 2105313.

5 T. Zhang, J. Han, T. Tang, J. Sun and J. Guan, Binder-free bifunctional SnFe sulfide/oxyhydroxide heterostructure electrocatalysts for overall water splitting, *Int. J. Hydrogen Energ.*, 2023, **48**, 4594-4602.

6 Z. Cai, A. Wu, H. Yan, Y. Xiao, C. Chen, C. Tian, L. Wang, R. Wang and H. Fu, Hierarchical whisker-on-sheet NiCoP with adjustable surface structure for efficient hydrogen evolution reaction, *Nanoscale*, 2018, **10**, 7619-7629.

7 J. Li, G. Wei, Y. Zhu, Y. Xi, X. Pan, Y. Ji, I. V. Zatovsky and W. Han, Hierarchical NiCoP nanocone arrays supported on Ni foam as an efficient and stable bifunctional electrocatalyst for overall water splitting, *J. Mater. Chem. A*, 2017, **5**, 14828-14837.

8 G. Zhao, B. Wang, Q. Yan and X. Xia, Mo-doping-assisted electrochemical transformation to generate CoFe LDH as the highly efficient electrocatalyst for overall water splitting, *J. Alloy. Compd.*, 2022, **902**, 163738.

9 J. Cen, L. Wu, Y. Zeng, A. Ali, Y. Zhu and P. K. Shen, Heterogeneous NiFeCoP/NF Nanorods as a Bifunctional Electrocatalyst for Efficient Water Electrolysis, *ChemCatChem*, 2021, **13**, 4602-4609.

10 W. Jin, J. Chen, H. Wu, N. Zang, Q. Li, W. Cai and Z. Wu, Interface engineering of oxygen-vacancy-rich $NiCo_2O_4$/NiCoP heterostructure as an efficient bifunctional electrocatalyst for overall water splitting, *Catal. Sci. Technol.*, 2020, **10**, 5559-5565.

11 J. Fang, X. Qian, J. Xia, B. Huang, G. He, Z. Zhang and H. Chen, Heterostructure engineering of self-supported bimetallic sulfide as an efficient bifunctional electrocatalyst for overall water splitting, *J. Alloy Compd.*, 2023, **937**, 168339.

12 L. Lin, R. Xin, M. Yuan, T. Wang, J. Li, Y. Xu, X. Xu, M. Li, Y. Du, J. Wang, S. Wang, F. Jiang, W. Wu, C. Lu, B. Huang, Z. Sun, J. Liu, J. He and G. Sun, Revealing Spin Magnetic Effect of Iron-Group Layered Double Hydroxides with Enhanced Oxygen Catalysis, *Acs Catal.*, 2023, **13**, 1431-1440.

13 J. Zhu, X. Zheng, C. Liu, Y. Lu, Y. Liu, D. Li and D. Jiang, Zinc and fluorine ions dual-modulated NiCoP nanoprism array electrocatalysts for efficient water splitting, *J. Colloid Interf. Sci.*, 2023, **630**, 559-569.
14 P. Wang, J. Qi, X. Chen, C. Li, W. Li, T. Wang and C. Liang, Three-Dimensional Heterostructured NiCoP@NiMn-Layered Double Hydroxide Arrays Supported on Ni Foam as a Bifunctional Electrocatalyst for Overall Water Splitting, *Acs Appl. Mater. Inter.*, 2020, **12**, 4385-4395.
15 C. Du, L. Yang, F. Yang, G. Cheng and W. Luo, Nest-like NiCoP for Highly Efficient Overall Water Splitting, *Acs Catal.*, 2017, **7**, 4131-4137.
16 Y. Hu, Z. Wang, W. Liu, L. Xu, M. Guan, Y. Huang, Y. Zhao, J. Bao and H.-m. Li, Novel Cobalt–Iron–Vanadium Layered Double Hydroxide Nanosheet Arrays for Superior Water Oxidation Performance, *Acs Sustain. Chem. Eng.*, 2019, **7**, 16828-16834.
17 L. Hu, L. Tian, X. Ding, X. Wang, X. Wang, Y. Qin, W. Gu, L. Shi and C. Zhu, p–d hybridization in CoFe LDH nanoflowers for efficient oxygen evolution electrocatalysis, *Inorg. Chem. Front.*, 2022, **9**, 5296-5304.
18 M. Hafezi Kahnamouei and S. Shahrokhian, Coupling NiCoS and CoFeS Frame/Cagelike Hybrid as an Efficient Electrocatalyst for Oxygen Evolution Reaction, *Acs Appl. Energ. Mater.*, 2022, **5**, 5199-5211.
19 D. Guo, H. Yu, J. Chi, Y. Zhao and Z. Shao, Cu_2S@NiFe layered double hydroxides nanosheets hollow nanorod arrays self-supported oxygen evolution reaction electrode for efficient anion exchange membrane water electrolyzer, *Int. J. Hydrogen Energ.*, 2023, DOI: 10.1016/j.ijhydene.2023.01.277.
20 J. Tian, Q. Liu, A. M. Asiri and X. Sun, Self-supported nanoporous cobalt phosphide nanowire arrays: an efficient 3D hydrogen-evolving cathode over the wide range of pH 0-14, *J. Am. Chem. Soc.*, 2014, **136**, 7587-7590.
21 G. Zhang, B. Wang, J. Bi, D. Fang and S. Yang, Constructing ultrathin CoP nanomeshes by Er-doping for highly efficient bifunctional electrocatalysts for overall water splitting, *J. Mater. Chem. A*, 2019, **7**, 5769-5778.
22 D. Rathore, S. Ghosh, J. Chowdhury and S. Pande, Fe-Doped $NiCo_2Se_4$ Nanorod Arrays as Electrocatalysts for Overall Electrochemical Water Splitting, *Acs Appl. Nano Mater.*, 2023, **6**, 3095-3110.
23 L. Chen, Y. Song, Y. Liu, L. Xu, J. Qin, Y. Lei and Y. Tang, NiCoP nanoleaves array for electrocatalytic alkaline H_2 evolution and overall water splitting, *J. Energy Chem.*, 2020, **50**, 395-401.
24 C. Hu, L. Zhang, Z. J. Zhao, A. Li, X. Chang and J. Gong, Synergism of Geometric Construction and Electronic Regulation: 3D Se-$(NiCo)S_x$ /$(OH)_x$ Nanosheets for Highly Efficient Overall Water Splitting, *Adv. Mater.*, 2018, **30**, e1705538.
25 V. H. Hoa, D. T. Tran, D. C. Nguyen, D. H. Kim, N. H. Kim and J. H. Lee, Molybdenum and Phosphorous Dual Doping in Cobalt Monolayer Interfacial Assembled Cobalt Nanowires for Efficient Overall Water Splitting, *Adv. Funct. Mater.*, 2020, **30**, 2002533.
26 X. Zhang, J. Fan, X. Lu, Z. Han, C. Cazorla, L. Hu, T. Wu and D. Chu,

Bridging NiCo layered double hydroxides and Ni_3S_2 for bifunctional electrocatalysts: The role of vertical graphene, *Chem. Eng. J.*, 2021, **418**, 129448.

27 R. Bose, V. R. Jothi, K. Karuppasamy, A. Alfantazi and S. C. Yi, High performance multicomponent bifunctional catalysts for overall water splitting, *J. Mater. Chem. A*, 2020, **8**, 13795-13805.

28 S. Wang, Y. Zhang, X. Deng, Z. Ma, R. Cheng, Z. Wan, J. Li and X. Wang, Rational construction of loosely packed nickel nanoparticulates with residual HCOO ligands derived from a Ni-MOF for high-efficiency electrocatalytic overall water splitting, *J. Mater. Chem. A*, 2023, **11**, 5222-5232.

29 C. He, Q. Liu, H. Wang, C. Xia, F. M. Li, W. Guo and B. Y. Xia, Regulating Reversible Oxygen Electrocatalysis by Built-in Electric Field of Heterojunction Electrocatalyst with Modified d-Band, *Small*, 2023, DOI: 10.1002/smll.202207474, e2207474.